99-431

Note: This is a preprint of a paper being submitted for publication. Contents of this paper should not be quoted nor referred to without permission of the author(s).

Alternative Gate Dielectrics on Semiconductors for MOSFET Device Applications

D. P. Norton, J. D. Budai, M. F. Chisholm, S. J. Pennycook, R. McKee*, F. Walker*, Y. Lee, and C. Park,

Solid State Division
Oak Ridge, National Laboratory,
Oak Ridge, TN 37831-6056

*Metals and Ceramic Division
Oak Ridge National Laboratory

Submitted to:
Proceedings of the 6th Intl. Workshop on Oxide Electronics
Dec. 6-7, 1999
College Park, MD

"The submitted manuscript has been authored by a contractor of the U.S. Government under contract DE-AC05-96OR22464. Accordingly, the U.S. Government retains a nonexclusive, royalty-free license to publish or reproduce the published form of this contribution, or allow others to do so, for U.S. Government purposes."

December 1999

Prepared by
Solid State Division
Oak Ridge National Laboratory
P.O. Box 2008
Oak Ridge, Tennessee 37831-6056
managed by
LOCKHEED MARTIN ENERGY RESEARCH CORP.
for the
U.S. DEPARTMENT OF ENERGY
under contract DE-AC05-96OR22464

Alternative Gate Dielectrics on Semiconductors for MOSFET Device Applications

D. P. Norton, J. D. Budai, M. F. Chisholm, S. J. Pennycook, , R. McKee, F. Walker*, Y. Lee, and C. Park*
Solid State Division
Oak Ridge, National Laboratory,
Oak Ridge, TN 37831-6056
*Metals and Ceramic Division
Oak Ridge National Laboratory
**Intel Corp.
Santa Clara, CA

We have investigated the synthesis and properties of deposited oxides on Si and Ge for use as alternative gate dielectrics in MOSFET applications. The capacitance and leakage current behavior of polycrystalline Y_2O_3 films synthesized by pulsed-laser deposition is reported. In addition, we also discuss the growth of epitaxial oxide structures. In particular, we have investigated the use of silicide termination for oxide growth on (001) Si using laser-molecular beam epitaxy. In addition, we discuss a novel approach involving the use of hydrogen to eliminate native oxide during initial dielectric oxide nucleation on (001) Ge.

1. INTRODUCTION

Metal/oxide/semiconductor (MOS) structures are key elements in microelectronic applications. **[1,2]** For silicon integrated circuit development, device architecture scaling relationships indicate that the capacitance/area requirement for the 0.1 µm linewidth technology will be on the order of 35 fF/µm^2. For a SiO_2-based capacitor structure, this corresponds to a dielectric oxide thickness of 1 nm. At this thickness, the magnitude of leakage current due to tunneling will be sufficiently high to make the usefulness of such devices doubtful. As such, there is significant interest in replacing SiO_2 with a material with a higher dielectric constant for use as the gate dielectric in Si-based MOSFET device structures. Figure 1 illustrates how film thickness constraints are relaxed for gate dielectrics with dielectric constants greater than that for SiO_2. One significant difficulty in satisfying this metric is in the tendency to form a thin SiO_2

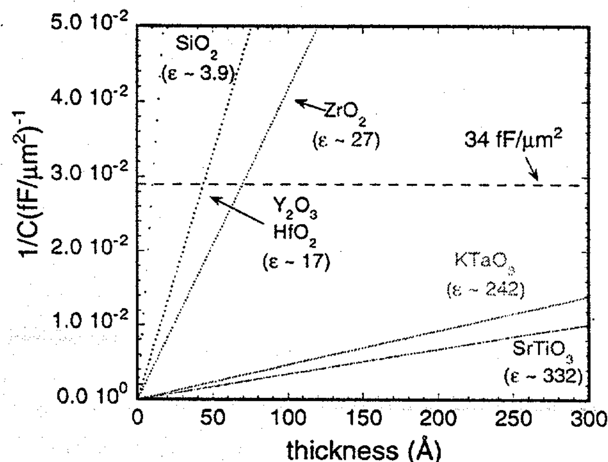

Figure 1 *Plot of inverse capacitance versus films thickness for various dielectric materials*

layer at the oxide/silicon interface. This directly limits the maximum capacitance/area that can be achieved. If, for example, a SiO_2 layer of only 10 Å forms at the interface due to a moderate reaction between the Si substrate and dielectric film, the metric can not be met. In addition to Si, MOS-type device structures are of interest for other semiconductor systems if a functional dielectric/semiconductor interface can be identified.

2. Polycrystalline Y_2O_3 on Si (001)

We have investigated the properties of polycrystalline Y_2O_3 films as a candidate for an alternative gate dielectric material. Yttria is attractive based on thermodynamic arguments regarding its stability in contact with silicon.[3] The films were deposited by pulsed laser deposition (PLD) using a KrF excimer laser. Oxide ceramic targets were used as the ablation sources. The Si (001) substrates were dipped in dilute HF/H_2O solution prior to loading for film deposition. Most of the effort focused on films with thickness of 5-10 nm. Deposition was carried out at a substrate temperature of 100-300°C. Capacitors were fabricated by e-beam evaporating 5 nm Cr/200 nm Au through a contact mask with 1 mm diameter holes. Back contacts were formed by evaporating Cr/Au on the back of the Si wafer following abrasion.

For deposited film thicknesses on the order of 5 to 10 nm, relatively high leakage currents make capacitance measurements rather difficult. In particular, the conventional equivalent circuits consisting of a capacitor with either a series or parallel resistance are not sufficient. In order to extract capacitance in the presence of a high leakage current, the complex impedance of the structures was modeled as a capacitor with both a series and parallel resistance. With three unknowns, this required measuring the complex impedance at two frequencies. Measurements were made at 50 and 100 kHz in order to derive the high frequency (100 kHz) capacitance, assuming that the elements within the model are frequency-independent for the frequency range considered.

Figure 2 shows the capacitance and leakage current behavior for a 12 nm thick Y_2O_3 film deposited on (001) Si. The substrate was p-type with a resistivity of 10-20 Ω-cm. There is a noticeable shift in the flat-band voltage that may result either from fixed charges in the oxide film or charges due to the e-beam evaporation of the metal gates. For the structure shown, the capacitance/area in accumulation is 14 fF/μm^2. Leakage current is $5x10^{-6}$ A/cm^2 at a gate bias of –1 volt, and $4x10^{-4}$ A/cm^2 at –2 Volts (accumulation). In the as-deposited films, there is significant dispersion in the C-V behavior. This may indicate ionic motion under bias due to oxygen vacancies within the Y_2O_3 matrix. This frequency dispersion can be minimized by

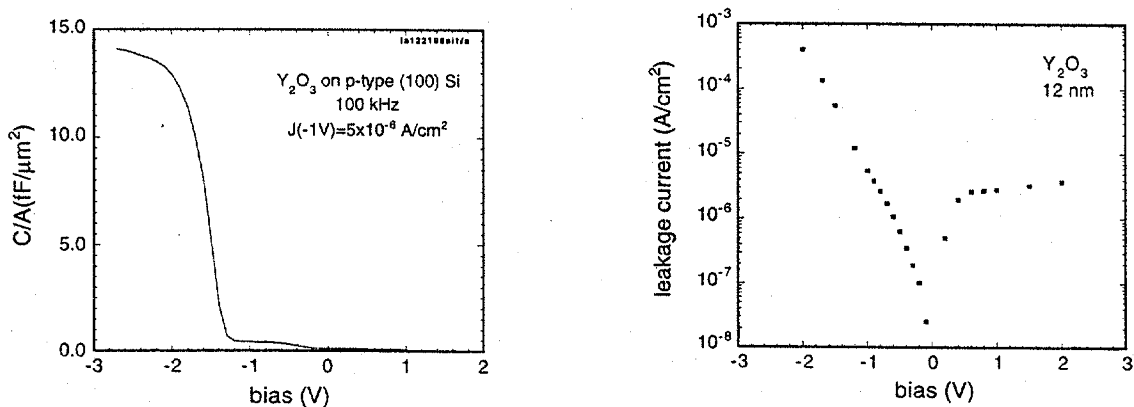

Figure 2 *C-V and leakage current behavior for 12 nm thick Y_2O_3 on (001) Si*

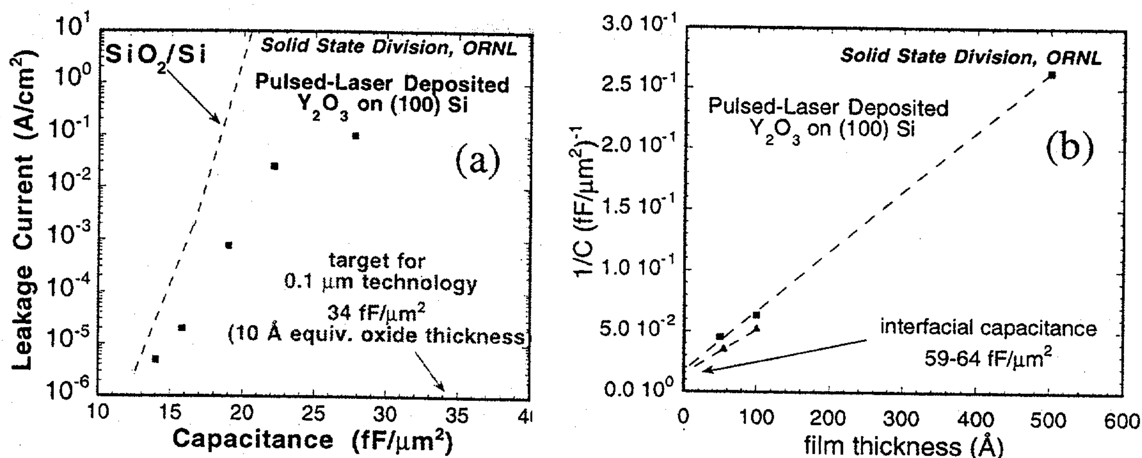

Figure 3 *Plot of leakage current versus areal capacitance (a) and inverse capacitance versus film thickness for polycrystalline Y_2O_3 films on p-type (001) Si.*

annealing in oxygen. Note that some hysteresis is also observed in the C-V with bias sweep. This has been attributed to the slow movement of mobile charges in the oxide at or near the oxide/semiconductor interface. Also, an anomaly in the 1 kHz C-V behavior appears upon annealing. This indicates the likely presence of interface charges at the oxide/semiconductor interface. The capacitance/area decreases with oxygen annealing presumably due to the growth of an interfacial SiO_2 layer. It is interesting to compare the performance of these deposited polycrystalline oxides with thermally grown SiO_2 on Si (001). Figure 3a) shows a plot of leakage current versus capacitance/area for a number of Y_2O_3 structures. For convenience, the behavior of SiO_2/ Si is shown. Note that the data for the Y_2O_3 films lies to the high-capacitance side of the SiO_2 /Si curve indicating promising performance. In addition, we have also plotted the inverse capacitance versus film thickness in Fig. 3b). The intercept at zero film thickness indicates the interfacial capacitance. For the Y_2O_3 films, this interfacial capacitance is ~ 60 fF/μm^2 which is encouraging in terms of ultimately achieving Y_2O_3 capacitors with high capacitance/area.

3. Epitaxial Oxides on (001) Si

The formation of epitaxial oxide structures on semiconductor surfaces represents an enabling development in the integration of electronic oxides on a semiconductor platform. This is particularly true for metal-oxide-semiconductor field effect transistor structures in which the oxide/semiconductor interface largely determines the properties of the device. Recently, there has been significant interest in the formation of epitaxial oxides on silicon for this application. One interesting approach is to terminate the Si(001) surface with an ordered silicide as an initial step in nucleating epitaxial oxides.[4] Silicide termination is achieved via high temperature epitaxy on an atomically-clean silicon surface. We have investigated the formation of $SrSi_2$ on Si (001) by laser molecular beam epitaxy (laser-MBE) using reflection high energy electron diffraction.

Laser molecular beam epitaxy simply refers to the growth of films by pulsed-laser deposition in a ultra-high vacuum environment. Laser-MBE has several attractive advantages over conventional MBE in that it is a truly digital film growth process with flux delivered to the substrate in a pulse-by-pulse mode. This not only allows for significant control of the film growth process, but also enables one to study the relaxation of the surface between flux delivery.

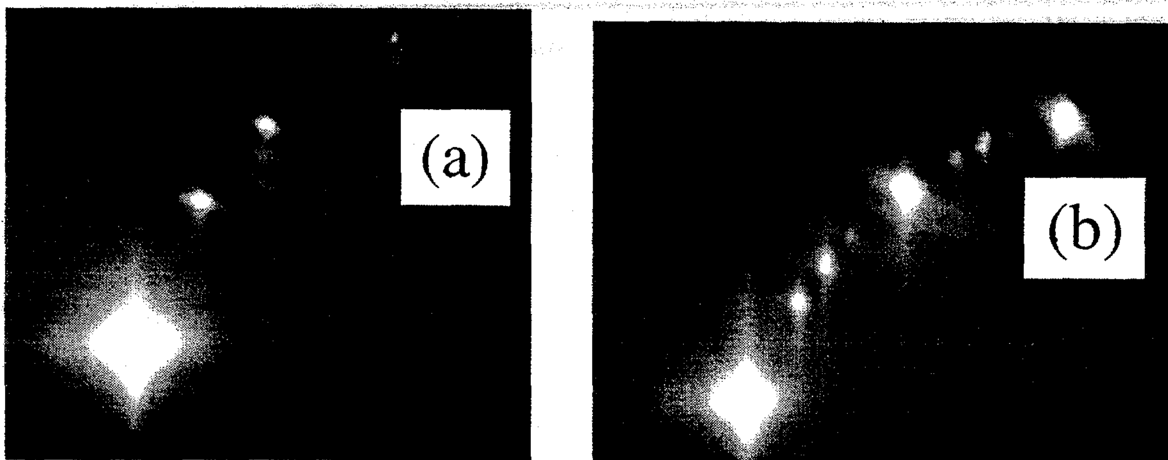

Figure 4 *RHEED images slightly off the Si (110) direction for clean (a) and sub-monolayer $SrSi_2$ covered surface*

L-MBE can utilize simple metal targets that are not intentionally heated, as is necessary for an evaporation cell. This greatly simplifies the hardware requirements for film growth. It also eliminates a heated source of potential impurities within the vacuum growth chamber. L-MBE also provides an energetic flux to the film growth surface which can impact film kinetics. The laser molecular beam epitaxy system used in this work consists of a UHV system with a base pressure of $4x10^{-10}$ Torr equipped with a liquid nitrogen-cooled shroud. 1" diameter Sr and Ba metal targets were mounted on a target carosel for in situ target selection. A KrF excimer laser was used as the ablation source. A laser energy of less than 0.4 J/cm^2 was used in order to minimize the density of ablation particulates. Metal flux was provided as a series of 5-10 shot bursts with a laser repetition rate of 100 Hz.

The Si(001) substrates were cleaned in trichloroethylene, acetone, and methanol in an ultrasonic bath. A UV-ozone treatment was then used to remove hydrocarbon contamination prior to film growth. The substrates were then loaded via a load-lock into the film growth chamber. The substrates were preannealed for ~ 30 minutes at 350°C before heating to 825-900°C for SiO_2 desorption as confirmed by a 2x1 reconstructed RHEED pattern. The substrates were then cooled to 650-725°C for deposition of Sr metal. Upon completion of silicide nucleation, the substrates were cooled to 100-200°C for additional metal and oxide growth.

Figure 4 shows the RHEED patterns from the substrate surface taken at various stages of the silicide formation. The images were acquired slightly off the Si(110) direction with an electron acceleration voltage of 10 kV. Fig. 4a) shows a clean 2x1 reconstructed Si(001) surface following the thermal desorption of a sacrificial SiO_2 layer at 850-900°C. Following desorption of the native oxide, the substrate is cooled to ~ 650-725°C for Sr deposition. Upon deposition of Sr, additional higher order reflections appear in the RHEED pattern as seen in Fig. 4b). This has been associated with formation of an ordered $SrSi_2$ phase on the Si surface. Upon deposition of additional Sr, the additional reflections disappear, resulting in the image identical to that shown in Fig. 4a). The appearance and disappearance of higher order spots indicates a 1/4 monolayer coverage of the Si(100) surface.[4] Additional Sr deposition does not result in a reappearance of the higher order reflections. It should be noted to the realization of this pattern was highly dependent on background contaminants. The use of a liquid nitrogen cooled shroud to reduce hydrocarbon impurities was essential to achieving reproducible results.

With a surface coverage of 1/4 monolayer, the substrate is cooled to 100-200°C for additional metal and subsequent oxide growth. Fig. 5 shows the RHEED patterns along the Si (110) and (100) directions achieved for an epitaxial (001) BaO layer growth on a $SrSi_2$ terminated Si surface at 150°C. The oxygen pressure during the initial oxide nucleation was

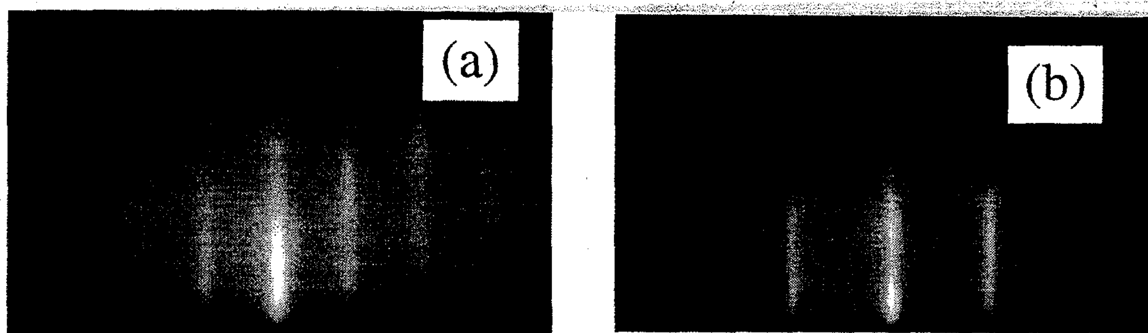

Figure 5 *RHEED images for BaO on Si(001) taken along the Si(110) (a) and (100) (b) directions.*

$5x10^{-8}$ Torr. It should be noted that the RHEED patterns were obtained over a limited region of the 1" diameter substrate presumably where near-ideal $SrSi_2$ sub-monolayer coverage occurred.

4. CeO_2 on (001) Ge by Hydrogen-Assisted Pulsed-Laser Deposition

Ge and SiGe alloys are attractive semiconductor materials for electronic applications, possessing higher carrier mobilities and thermal conductivities than that of silicon. Germanium possesses a simple cubic crystal structure with $\mu_n = 3900$ cm^2/V-sec, $\mu_p = 1800$ cm^2/V-sec, and a thermal conductivity of 0.6 W/cm-K. Unfortunately, the native germanium oxides are not suitable for MOS-type device structures.**[5,6]** The formation of stable metal oxides on Ge could prove instrumental in the development of Ge and/or SiGe alloy integrated circuits. In addition, a method to form oxides that are epitaxial on these semiconductors would enable the integration of various epitaxial oxide materials and device structures with semiconductor electronics by providing a crystalline oxide template for additional epitaxial oxide film growth.

We report on the epitaxial growth and properties of CeO_2 on (001) Ge using pulsed-laser deposition. Hydrogen is introduced as a background gas during the film nucleation in order to eliminate the native GeO_2 on the Ge surface and achieve epitaxy.**[7,8]** The use of hydrogen greatly relaxes vacuum requirements needed for the formation of a GeO_2-free surface. Using this approach, (001)-oriented CeO_2 thin films were obtained on the (001) Ge surface. The resulting metal oxide/semiconductor interface is atomically abrupt, with no apparent native oxide present at the semiconductor /metal oxide interface. These results differ from that observed for CeO_2 on (001) Si, where the film is (110)-oriented with significant SiO_2 formation at the film/substrate interface.**[9-11]**

The deposition of (001) epitaxial cerium oxide on single crystal Ge (001) was performed by pulsed-laser deposition using a KrF excimer laser. Single crystal (001) Ge substrates were cleaned by successive rinsing in trichloroethylene, acetone, and methanol, followed by rinsing in deionized water. The native oxide was then removed by a 30 sec dipping in a 1:10 HF:H_2O solution. The substrate was blown dry with dry nitrogen and mounted on the heater platen using silver paint. The sample was loaded into the vacuum chamber for pulsed-laser deposition of the oxide film. The chamber was evacuated to an initial base pressure that ranged from $5x10^{-6}$ Torr to $2x10^{-9}$ Torr. The mounted Ge substrate was annealed in vacuum at 350°C for 2-12 hrs in order to decompose the organic binder in the silver paint. Prior to heating, the ablation target was in situ cleaned by laser ablation with a shutter between the substrates and ablation target.

In order to minimize or eliminate any native germanium oxide on the substrate surface prior to growth, hydrogen gas was introduced into the chamber to a sufficient pressure such that the

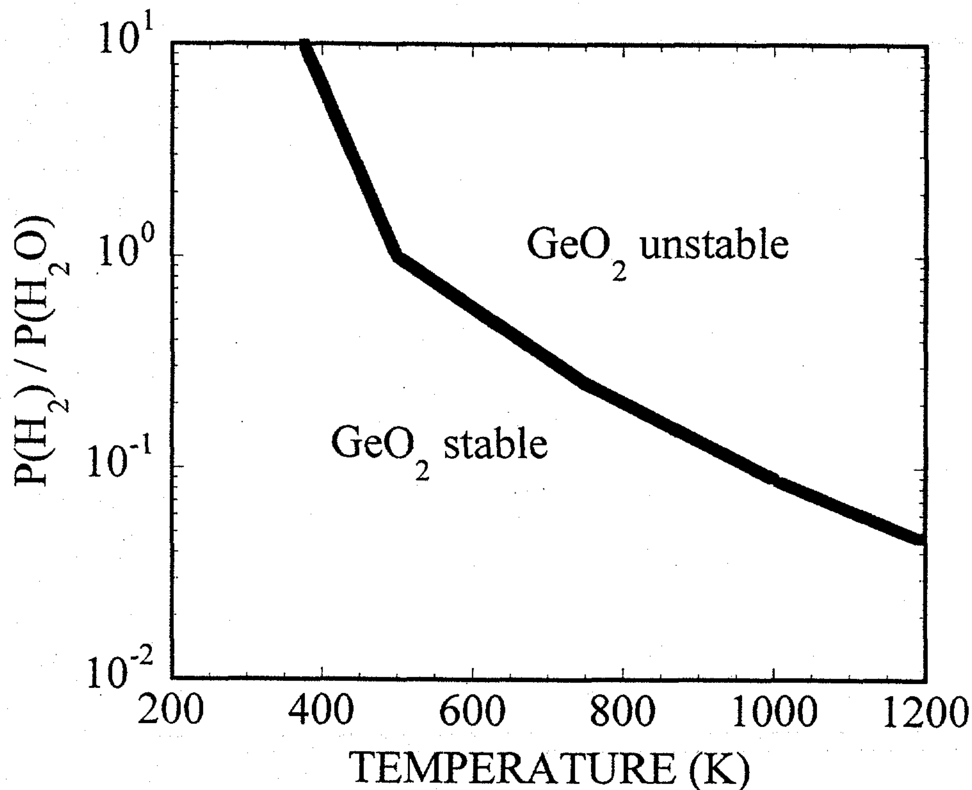

Figure 6 *Plot showing GeO_2 stability line with respect to the ratio of hydrogen gas to water vapor. The conditions for which GeO_2 is unstable are explicitly denoted.*

ratio of hydrogen to water vapor partial pressure $P(H2) / (P(H2O)$ was approximately at or above the $GeO2$ stability curve at the anticipated oxide film growth temperature as shown in Fig. 6. This curve was derived from Ellingham diagrams for oxide materials.**[12,13]** The oxide stability line can be estimated from the temperature-dependent Gibbs free energy of the chosen native oxide when compared to the H_2O/H_2 equilibrium behavior. Depending on the anticipated metal oxide deposition temperature, the GeO_2 instability criterion translates into a value of $P(H_2)/P(H_2O) > 0.04$, preferably greater than 1.0. As a practical matter, the base pressure of the vacuum systems consists mostly of H_2O.

For the experiments reported here, a flow of 4% $H2$ / 96% Ar was introduced into the chamber with the $H2/Ar$ pressure ranging from 10^{-5} to 10^{-1} Torr, depending on the base pressure. For example, an H_2/Ar pressure of 0.1 Torr yields a hydrogen partial pressure of $4x10^{-3}$ Torr, and a value of $P(H_2)/P(H_2O)$ of $8x10^2$ for a base pressure of $5x10^{-6}$ Torr. The substrate was then heated to the growth temperature in the 4% $H2$ / 96% Ar background. As the substrate is heated, the hydrogen reduces any $GeO2$ that resides or forms on the substrate surface, resulting in the gas-phase etching of the native oxide. The final growth temperature must be consistent with the requirement that the conditions (temperature, water vapor partial pressure, hydrogen partial pressure) be above the $GeO2$ stability line where the formation of $GeO2$ is thermodynamically unfavored. Under these conditions, a metal oxide material that is stable for the chosen temperature/water vapor/hydrogen conditions can be deposited onto the heated substrate by means of pulsed-laser deposition. This oxide material should be thermodynamically stable in contact with Ge.[3] Cerium oxide satisfies this criterion.

After heating to the selected growth temperature, a CeO_2 film was deposited on the Ge surface. The KrF excimer laser energy density was ~ 1.5 J/cm^2 with a laser repetition rate of 1 Hz. These conditions yielded a deposition rate of ~ 0.1 nm/laser pulse when using a pressed and sintered CeO_2 ablation target. Both the metal cation and oxygen atoms are provided by laser ablation as short, discreet pulses. Between the laser pulses, the metal oxide / semiconductor system can relax to the conditions that thermodynamically favor instability of the native oxides. After the initial film nucleation, additional CeO_2 could be deposited on the initial oxide film template using deposition conditions that do not necessarily coincide with the requirements of GeO_2 thermodynamic instability as outlined for the template oxide layer, thus allowing the CeO_2 stoichiometry to be controlled. After film growth, the germanium substrate was typically cooled in vacuum.

X-ray diffraction data were taken for a series of 50 nm thick CeO_2 films on (001) Ge grown at temperatures ranging from 450 to 775°C. The CeO_2 films were deposited with $P(H_2) = 4x10^{-7}$ Torr and a base pressure = $2x10^{-9}$ Torr. Approximately 5 nm was deposited in the presence of hydrogen. The remaining 45 nm of CeO_2 was deposited with no hydrogen flow. For temperatures greater than 550°C, only the (001) orientation is observed. In-plane XRD scans confirm that the CeO_2 films are in-plane aligned. Note that some broadening in 2θ is observed at the lower growth temperature, indicating that strain is present in the film.

In addition to x-ray diffraction, the properties of the CeO_2 / Ge interface were investigated using high-resolution scanning transmission electron microscopy (STEM). Cross-section images reveal that CeO_2 films deposited at 750°C possesses a 3D island-like morphology that is faceted, with extended defects (pinholes) extending to the substrate at some of the faceted boundaries. Disruption of the CeO_2/Ge interface in the form of etched holes or amorphous material was evident in the proximity of these defects. Between the defects, the CeO_2/Ge interface is atomically abrupt and free of GeO_2. At slightly lower temperatures, faceting is significantly diminished. Figure 7 shows a cross-section Z-contrast STEM image of a CeO_2 film that was grown at 650°C. The absence of an amorphous native oxide layer at the interface differs from that observed for CeO_2 films on Si, where significant SiO_2 is observed at the film/substrate interface. The fact that GeO_2 is thermodynamically less stable than SiO_2 suggests that the formation of GeO_2 at the interface should be less likely.

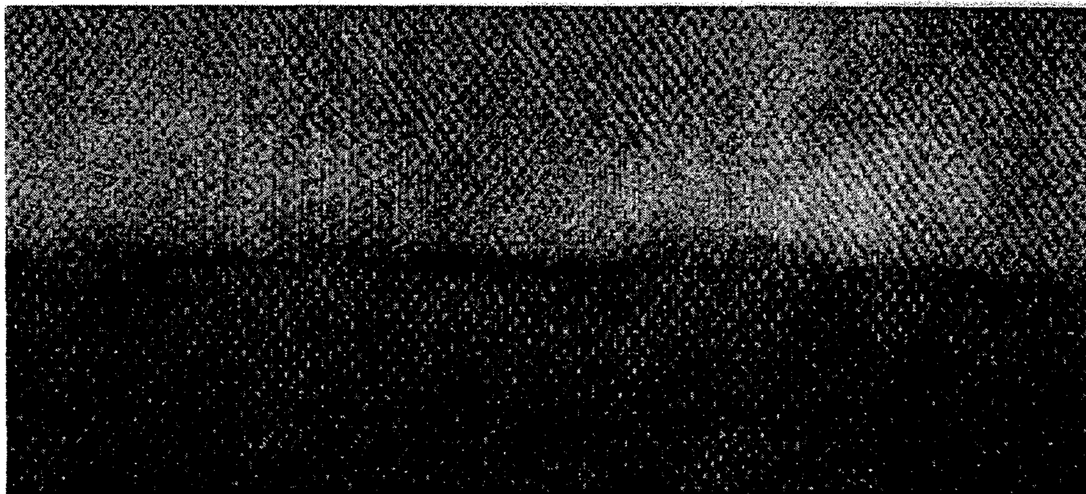

Figure 7 *High resolution STEM image of the atomically abrupt CeO_2/Ge crystalline interface.*

5. CONCLUSIONS

In conclusion, we have investigated the synthesis and properties of moderate to high- k dielectric materials on Si and Ge for MOSFET applications. Polycrystalline yttria/Si interfaces suffer from charge trapping and relatively high interface trap states, although the capacitance/leakage current behavior is encouraging. The termination of Si(001) with strontium silicide for subsequent growth of epitaxial oxide thin films have also been examined. Laser-MBE has been successfully used to form both the ordered silicide layer and epitaxial alkaline earth oxides. In addition, the growth of (001) epitaxial CeO_2 on a (001) Ge surface using pulsed-laser deposition in a hydrogen ambient has been realized. By using hydrogen to eliminate GeO_2 from the surface during film nucleation, a CeO_2 / Ge interface that is essentially free of GeO_2 can be formed. The use of hydrogen to promote the epitaxial growth of oxides on semiconductor surfaces should be applicable not only to CeO_2 on Ge by PLD, but to other material systems and physical vapor deposition techniques. The resulting epitaxial metal oxide film should be useful as a crystalline oxide template for subsequent growth of additional epitaxial oxide layers on the semiconductor surface. These structure may prove useful for numerous electronic and optoelectronic devices, including metal-oxide-semiconductor field-effect transistors, random-access memory devices, and optical waveguide structures.

The authors would like to acknowledge Gang Bai and Baylor Triplett of Intel Corp. for many useful discussions. This research was sponsored by the Office of Sciences and the Office of Power Technology, U.S. Department of Energy under contract No. DE-AC05-96OR22464 with Lockheed Martin Energy Research Corp.

REFERENCES

1. S. K. Ghandhi, "VLSI Fabrication Principles: Silicon and Gallium Arsenide," John Wiley & Sons, New York, 1983.
2. E. H. Nicollian and J. R. Brews, "MOS (Metal Oxide Semiconductors) Physics and Technology," John Wiley & Sons, New York, 1982.
3. K. J. Hubbard and D. G. Schlom, J. Mater. Res. **11**, 2757-2776 (1996).
4. R. A. McKee, F. J. Walker, and M. F. Chisholm, Phys. Rev. Lett. **81**, 3014 (1998).
5. K. M. Horn, E. Chason, J. Y. Tsao, J. A. Floro, S. T. Picraux, Surface Science **320**, 174-184 (1994).
6. L. Surnev and M. Tikhov, Surface Science **123**, 505-518 (1982).
7. D. P. Norton, A. Goyal, J. D. Budai, D. K. Christen, D. M. Kroeger, E. D. Specht, Q. He, B. Saffian, M. Paranthaman, C. E. Klabunde, D. F. Lee, B. C. Sales, and F. A. List, Science **274**, 755 (1996).
8. M. Paranthaman, A. Goyal, F. A. List, E. D. Specht, D. F. Lee, P. M. Martin, Q. He, D. K. Christen, D. P. Norton, J. D. Budai, and D. M. Kroeger, Physica C **275**, 266 (1997).
9. S. H. Jang, D. Jung, and Y. Roh, J. Vac. Sci. Technol. B **16**, 1098 (1998).
10. H. Koinuma, J. Nagata, T. Tsukahara, S. Gonda, and M. Yoshimoto, Appl. Phys. Lett. **58**, 2027 (1991).
11. T. Inoue, T. Ohsuna, L. Luo, X. D. Wu, C. J. Maggiore, Y. Yamamoto, Y. Sakurai, and J. H. Chang, Appl. Phys. Lett. **59**, 3604 (1991).
12. T. B. Reed, "Free Energy of Formation of Binary Compounds," (MIT Press, Cambridge, MA, 1971).
13. P. W. Atkins, "Physical Chemistry", (Oxford University Press, Oxford, 1982)